# Phonons in GdS—Raman scattering of an fcc metal

G. Güntherodt, P. Grünberg,* E. Anastassakis,† M. Cardona, H. Hackfort,* and W. Zinn*
*Max-Planck-Institut für Festkörperforschung, 7 Stuttgart 80, Federal Republic of Germany*
(Received 20 May 1977)

Metallic, fcc GdS was investigated by means of Raman scattering. First- and second-order Raman scattering was observed and identified by the dependence on temperature and defect concentration. Particular consideration was given to the effect of sample stoichiometry on the Raman spectra. The symmetry-forbidden first-order scattering is found to be defect induced, in contrast to the defect-independent, allowed, second-order scattering. The observed defect-induced one-phonon density of states was assigned to acoustical and optical branches. Raman scattering of GdS provides information about the phonon spectrum which cannot be obtained from neutron scattering or infrared spectroscopy. The antiferromagnetic order of GdS is found to have no effect on the Raman scattering, which is attributed to the nonresonant excitation of the $4f^7$ states at about 7 eV below the Fermi level.

## I. INTRODUCTION

The monochalcogenides of the rare earths ($R$) represent an interesting class of cubic materials, comprising magnetic semiconductors and metals. Monochalcogenides of divalent $R$ ions are semiconducting, whereas metallic for trivalent $R$ ions. Among the latter are the antiferromagnetic gadolinium monochalcogenides Gd$X$ ($X$ = S, Se, Te), which crystallize in the fcc crystal structure. Their optical properties have been investigated extensively in recent years.[1-3] However, the metallic character of Gd$X$ prevents the study of the phonons by means of infrared spectroscopy. Also, neutron scattering cannot provide this information because of the extremely large neutron absorption cross section of the natural Gd isotope ($\sigma = 20000 \times 10^{-24}$ cm$^2$ for $Gd^{157}$, compared to, e.g., $\sigma = 0.13 \times 10^{-24}$ cm$^2$ for Al).[4] On the other hand, Raman scattering (RS) of cubic and metallic Gd$X$ does, at first glance, not appear to be an appropriate tool either. First-order RS in a perfect lattice with rocksalt structure is forbidden by symmetry. Furthermore, RS in metals meets in general with the difficulty of a small penetration depth of the light. Hence, the scattering volume and the corresponding efficiency are strongly reduced. In this respect, however, we could fortunately profit from two advantageous features of Gd$X$. First, the plasma reflection edge of Gd$X$ is positioned in the visible region of the spectrum.[1-3] Thus, unlike standard metals, the penetration depth of the radiation of conventional lasers is reasonably high in Gd$X$ for laser frequencies above the plasma edge. Second, the pronounced defect structure of Gd$X$[1-3,5] provides the possibility for the symmetry-forbidden first-order RS to become allowed.

In this paper we present, as an extension of our previous work on RS of GdS,[6] a systematic study with particular consideration of the stoichiometry of the samples. To elucidate the origin of the scattering mechanism, we attempt to correlate changes in stoichiometry and conduction-electron concentration[3] with characteristic features of the Raman spectra. Therefore, the measurements have also been extended towards low temperatures in order to distinguish between first-order and second-order scattering. The low-temperature measurements in turn are also of importance in searching for magnetic excitations and for the influence of the antiferromagnetic order on the RS of GdS. Moreover, antiferromagnetic GdS provides a good test of the importance of the localized and magnetic $4f$ states as initial states in spin-dependent phonon RS[7] of rare-earth compounds, especially in Eu$X$ ($X$ = O, S, Se, Te).[8,9] In Eu$X$ the localized $4f$ states are positioned in the vicinity of the Fermi energy, $E_F$, whereas about 7 eV below $E_F$ in GdS.[10] Hence, with presently used gas-laser lines (~1.5–4 eV), only the $4f$ states in Eu$X$, but not in GdS, are subject to resonant optical excitation in RS experiments. Another interesting link between RS of GdS and of its semiconducting counterpart EuS exists through the investigation of the solid-solution system $Eu_{1-x}Gd_xS$ ($0 \leq x \leq 1.0$) and the calculated phonon dispersion of EuS.[9]

A brief review of the electronic structure of GdS is given in Sec. II. Sample preparation and experimental results on RS of GdS are presented in Sec. III, followed by a discussion in Sec. IV.

## II. ELECTRONIC STRUCTURE OF GdS

Some basic information about the electronic structure of GdS has been provided by photoemission[11,12] and optical experiments.[1-3] Gadolinium has the electronic configuration $[Xe]4f^7 5d^1 6s^2$. In compounds, such as GdS, it prefers the trivalent ionization state because of the very stable half-filled $4f$ shell. Hence one electron per $Gd^{3+}$ ion is

TABLE I. Interpolated data of the samples used in this work. The reflectivity minima $R_{min}$ associated with the plasma reflection edge of $Gd_xS$ ($x = 1.0, 0.8, 0.7$) serve as a basis for interpolating composition and conduction-electron concentration $n_{el}$ of the data of Ref. 3.

| This work (interpolated) | Ref. 3 | $R_{min}$ (eV) | $10^{22} n_{el}$ ($cm^{-3}$) | Color | Sample |
|---|---|---|---|---|---|
| | $GdS_{0.94}$ | 3.4 | 2.63 | | |
| $Gd_{1.0}S_{1.0}$ | | 3.2 | 2.35 | Gold | Single crystal |
| | $Gd_{0.94}S$ | 3.0 | 2.12 | | |
| $Gd_{0.8}S$ | | 2.45 | 1.8 | Red | Single crystal |
| $Gd_{0.7}S$ | | 2.15 | 1.6 | Blue | Thin film |

transferred to the $(5d, 6s)$ states, which form the conduction band. The $5d$ orbitals are split by the cubic crystal field into zone-center $t_{2g}$ and $e_g$ states. The Fermi energy $E_F$ is positioned within the partially filled $5dt_{2g}$-derived subband. The $S(3p)$ orbitals form the valence band which is well separated from the $(5d, 6s)$ conduction band.[11,12] The onset of interband transitions from the $p$ valence band into empty $(5d, 6s)$ states above $E_F$ depends on stoichiometry. It occurs at 3.1 eV for $Gd_{0.94}S$ and at 3.5 eV for $GdS_{0.94}$.[3] The defect structure of GdS (cation and/or anion vacancies) manifests itself in an unusual change in conduction-electron concentration without significantly changing the lattice parameters or the structure of the lattice. The plasma reflection edge is positioned in the visible region of the spectrum due to a strong coupling between plasmons and interband transitions.[3] Shifts in the position of this edge due to changes in conduction-electron concentration cause a drastic change in the color of the samples. This change can range from bright lustrous gold[3] for $GdS_{0.94}$ to dark blue for $Gd_{0.7}S$ (Table I and Fig. 1). Two representative reflectivity spectra of samples used in this work are shown in Fig. 1. The reflectivity minimum at 3.2 eV of the gold-colored sample ($Gd_{1.0}S_{1.0}$) indicates a composition of GdS close to 1:1 by comparison with previous optical data.[3] The reflectivity spectrum of the blue-colored sample ($Gd_{0.7}S$), with its minimum at 2.15 eV and a maximum at 2.9 eV, is very similar to that of GdTe.[3] The latter sample is also blue in color and has its onset of interband transitions at 2.0 eV.[3] With the laser lines used in this investigation (2.4–2.7 eV), we are in a region of about 20% reflectivity. According to the optical constants obtained by Kramers-Kronig analysis of the reflectivity[3] the penetration depth of the light in this region is $d \sim 200$–$400$ Å. For GdS a quantitative correlation has been established between the reflectivity minimum, associated with the plasma reflection edge, and the stoichiometry of the sample.[3] The samples used in this work have been characterized primarily on the basis of the position in energy of these reflectivity minima. The composition and conduction-electron concentration of our samples have been determined by interpolating previous data[3] as shown in Table I. This is sufficient for the purpose of our present work in order to correlate trends in RS with those in composition and conduction-electron concentration of the samples.

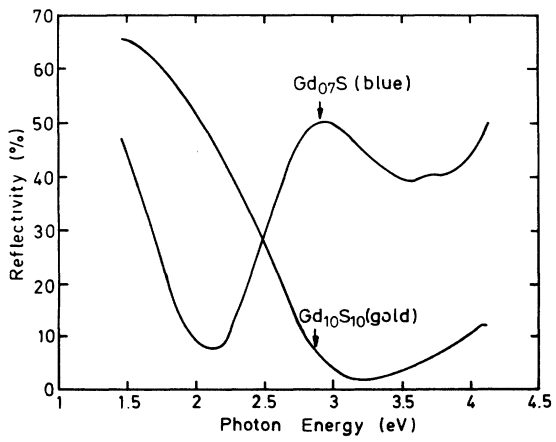


FIG. 1. Room-temperature reflectivity of $Gd_{1.0}S_{1.0}$ (gold, single crystal) and $Gd_{0.7}S$ (blue, thin film).

## III. EXPERIMENTAL RESULTS

Some general aspects of crystal growth of Gd monochalcogenides have been outlined in Ref. 3, including references cited therein. The GdS single crystals used in the present experiments (Table I) were grown from the melt. Gd and S in stoichiometric ratio were sealed under vacuum in a tungsten crucible and then heated to 2500 °C for 15 min. The melt was slowly cooled down to 2080 °C at a rate of 25 °C/h and then rapidly cooled down to 1000 °C. Thus crystals of an average length of 3 mm were obtained. These crystals were also used for the preparation of thin films by current heating of a tungsten boat. The evaporation occured onto glass substrates, kept at 490 °C. During evaporation the pressure rose from about $5 \times 10^{-9}$ Torr to approximately $10^{-5}$ Torr. After deposition, the films were annealed for 1 h at $10^{-8}$ Torr and 350 °C. The films had deep blue color. Their structure was examined by transmission electron microscopy of small carbon films which had been exposed to the vapor beam simultaneously with the glass substrates. In addition to the rocksalt structure of GdS, evidence for small amounts of additional structures was found.

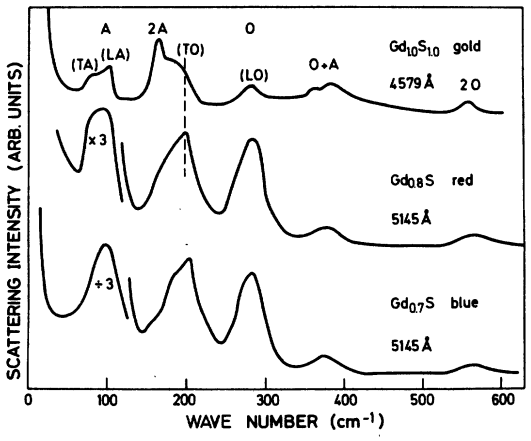


FIG. 2. Raman spectra of $Gd_{1.0}S_{1.0}$ (gold, single crystal), $Gd_{0.8}S$ (red, single crystal), and $Gd_{0.7}S$ (blue, thin film) at 300 K.

The residual material left in the tungsten boat after evaporation had orange to red color, parts of which showed the cleavage properties typical of GdS. One such cleavage plane was used in our measurements and is referred to as red sample (Table I and Fig. 2).

Our measurements were performed by means of conventional experimental techniques. Most of the $Ar^+$ laser lines were used. Representative room-temperature spectra of $Gd_{1.0}S_{1.0}$, $Gd_{0.8}S$ and $Gd_{0.7}S$ are shown in Fig. 2. The spectra in Fig. 2 as well as those in Figs. 3–5 have been redrawn from the original data by omitting the noise. To get an idea of the signal-to-noise ratio in our measurements and to demonstrate the significance of spectral features, the noise level has been reproduced in Fig. 7. As already mentioned, first-order RS of GdS is forbidden by symmetry in a perfect crystal. However, for all samples we observe detailed and similar structures in the range from 50 to 600 $cm^{-1}$. Apart from some changes in intensity and width of the bands, all structures of the three different samples in Fig. 2 appear around the same frequencies: Between 70 and 120 $cm^{-1}$ ($A$) and 140 and 240 $cm^{-1}$ ($2A$), around 285 $cm^{-1}$ ($O$), between 350 and 410 $cm^{-1}$ ($O+A$) and around 565 $cm^{-1}$ ($2O$). The meaning of the symbols will be explained in Sec. IV. In this section these symbols are used just for the sake of convenience. However, it should be mentioned, of course, that $O$ stands for optical, $A$ for acoustic and that the notations $2A$, $O+A$ and $2O$ denote possible overtones and combinations of the corresponding bands. The $A$ and $O$ bands show a much stronger intensity for the samples with cation deficiencies ($Gd_{0.8}S$, $Gd_{0.7}S$) than for $Gd_{1.0}S_{1.0}$. At the same time, the broad $2A$ band shows a small increase in intensity with increasing cation deficiencies, but most significantly a change in its shape. The $O+A$ band of $Gd_{1.0}S_{1.0}$ shows a double-peak structure similar to that of the $A$ band. Correspondingly, the disappearance of the double-peak structure in the A band of $Gd_{0.8}S$ and $Gd_{0.7}S$ is also observed for their $O+A$ bands. On the other hand, the intensity of the $O+A$ and $2O$ bands is practically unaffected by changes in stoichiometry of the samples.

Here the question arises as to whether deviations from stoichiometry and/or the concurrent change in carrier concentration (Table I) are responsible for the systematic changes in the spectra of the various samples of different compositions. In order to clarify this point, we have attempted to characterize the detailed features of the spectra in Fig. 2 and the underlying scattering mechanism. Therefore, we have performed measurements as a function of temperature. This, in turn, is also of importance in studying the influence of magnetic order on the RS. Figure 3 shows the Raman spectra of a $Gd_{1.0}S_{1.0}$ single crystal for various temperatures between 300 K and 10 K. All bands show a small, continuous shift towards higher frequencies upon cooling below room temperature. While the intensity of the $O$ band is practically unaffected by changes in temperature, the $A$ band decreases in intensity by about a factor of 3 upon cooling from 300 to 10 K. Over the same temperature range the most striking decrease in intensity by about a factor of 9 is observed for the $2A$ band upon cooling. At 10 K this band has been reduced to an intensity about that of the $A$ and $O$ bands. A very similar behavior is found for $Gd_{0.7}S$ in Fig. 4: the

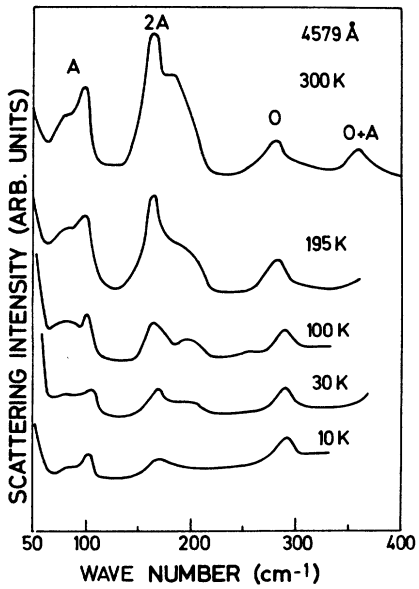


FIG. 3. Raman spectra of $Gd_{1.0}S_{1.0}$ (gold, single crystal) at different temperatures.

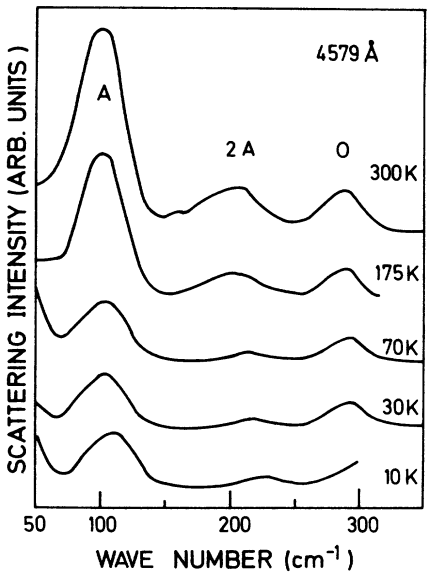


FIG. 4. Raman spectra of $Gd_{0.7}S$ (blue, thin film) at different temperatures.

changes in intensity upon cooling are approximately the same as for the corresponding bands in Fig. 3. The decrease in intensity of the $A$ and $2A$ bands in Figs. 3 and 4 is observed already for $T \gg T_N$ ($\simeq$50 K) and thus does not coincide with the onset of magnetic order or even short-range order. The spectra for $T \lesssim T_N$ in Figs. 3 and 4, measured in zero external magnetic field, do not show any indication of additional structure or shifts associated with the onset of antiferromagnetic order or due to magnetic excitations. This is, at first glance, somewhat surprising in view of the relatively high $T_N \simeq 50$ K and the very recent observations of spin-dependent phonon RS in metamagnetic EuSe,[13] and antiferromagnetic EuTe.[8,9] In the latter two cases it has been shown that in the region of antiferromagnetic order ($T \lesssim T_N$) the RS process is determined by the symmetry of the magnetic unit cell, whose dimensions can be an integer multiple of the chemical unit cell.

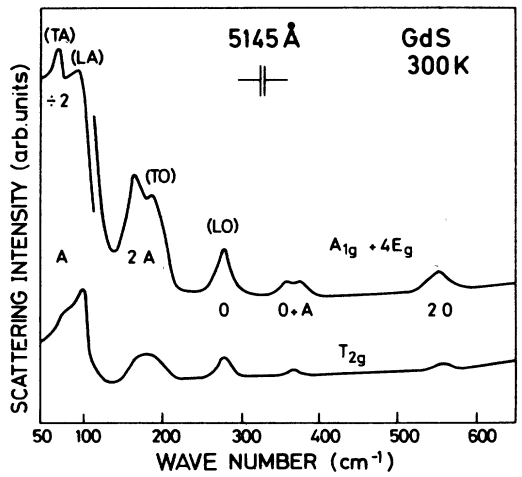


FIG. 5. Polarization dependence of the Raman scattering of a single-crystal (100) plane of $Gd_{1.0}S_{1.0}$ at 300 K in $x(yy)\bar{x}$ ($A_{1g}+4E_g$) and $x(yz)\bar{x}$ ($T_{2g}$) scattering configuration.

The polarization dependence of the RS of a (100) plane of a $Gd_{1.0}S_{1.0}$ single crystal is shown in Fig. 5 for $T = 300$ K. The most dominant contribution to the scattering is found in the $x(yy)\bar{x}$ configuration ($A_{1g}+4E_g$), compared to a relatively small contribution from the $T_{2g}$ Raman tensor component in $x(yz)\bar{x}$ configuration.

## IV. DISCUSSION

GdS is a metallic compound with an unusual change in conduction-electron concentration due to deviations from stoichiometry. A 30% change in conduction-electron concentration accompanies a 30% increase in Gd vacancies from $Gd_{1.0}S_{1.0}$ to $Gd_{0.7}S$. However, our notation $Gd_{1.0}S_{1.0}$ does not necessarily mean that the crystal is indeed stoichiometric and perfect. Obviously, the assignment of a $Gd_{1.0}S_{1.0}$ composition to our gold sample by interpolating previous optical data is not very accurate. Furthermore, chemical and microprobe analysis[3] can only provide a Gd to S ratio. Hence, without measuring the density of the material, a 1:1 composition can also imply equal amounts of vacancies in either sublattice. Consequently, the weak structure in the Raman spectrum of $Gd_{1.0}S_{1.0}$ in Figs. 2, 3, 5, and 7 can possibly have its origin in a defect-induced first-order RS, besides structure due to allowed second-order RS. The possibility of the latter being due to a second-order process in which a phonon and an electron-hole pair are simultaneously created cannot be discarded.

A band analogous to the $A$ band in Fig. 2 is also observed around similar frequencies in EuS, $Eu_{1-x}Gd_xS$, $Eu_{1-x}Sr_xS$,[9] and SmS.[9,14] On the basis of the calculated phonon dispersion and the derived, unweighted one-phonon density of states of EuS [9,15] and SmS,[9,14] there is strong evidence that the $A$ band in Fig. 2 corresponds to the density of states of acoustic phonons. The two peaks of the $A$ band of $Gd_{1.0}S_{1.0}$ in Figs. 2 and 3 at 83 $cm^{-1}$ and 103 $cm^{-1}$, respectively, agree well with the two prominent peaks of TA phonons at 84 $cm^{-1}$ and of LA phonons at 116 $cm^{-1}$ in the density of acoustic phonons calculated for EuS.[9,15] Hence we conclude that the $A$ band of $Gd_xS$($x = 1.0, 0.8$ and 0.7) in Fig. 2 occurs because of defect-induced first-order Raman scattering. This is strongly supported by alloying EuS with GdS.[9] The $A$ band of EuS becomes increasingly more pronounced with increas-

ing Gd concentration in the $Eu_{1-x}Gd_xS$ solid-solution system. Besides possible clustering effects, the $Gd^{3+}$ ions act as defects due to their different ionic radius $r_{Gd}3+ = 1.02$ Å, compared to $r_{Eu}2+ = 1.12$ Å. Analogously, the *A* band of $Gd_{1.0}S_{1.0}$ in Fig. 2 becomes more intense with increasing cation deficiencies. Further support for the first-order nature of the *A* band is given by its Stokes–anti-Stokes ratio and by the relatively weak temperature dependence of its integrated intensity in Figs. 3 and 4. The latter is in good agreement with the calculated temperature dependence of the Bose factor of first-order Stokes scattering of a mode at, e.g., 80 $cm^{-1}$ as shown by the experimental points (+) in Fig. 6. The breakdown of translational and inversion symmetry due to defects in a perfect cubic lattice relaxes the $\vec{k}$-selection rule. First-order RS becomes allowed throughout the Brillouin zone. Consequently, we conclude that the *A* band in Figs. 2–5 and 7 represents the density of states of acoustic phonons.

An increase in intensity with Gd defects or vacancies similar to that found for the *A* band is also found for the *O* band around 285 $cm^{-1}$ in Fig. 2. The defect-induced origin of the scattering of the *O* band is also supported by comparing cleaved and polished surfaces of a single crystal as shown in Fig. 7. Clearly, the weak *O* band of the cleaved $Gd_{1.0}S_{1.0}$ single crystal becomes more intense upon polishing its surface. By doing so, one introduces additional defects. Scattering due to these surface

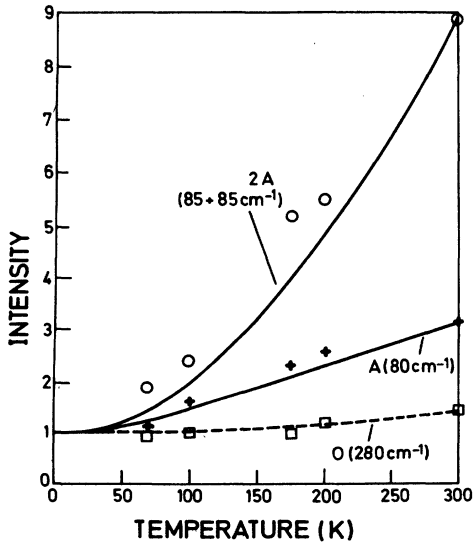


FIG. 6. Calculated temperature dependence of the intensity of Stokes scattering of first-order $(n_1+1)$ and second-order, $(n_1+1)(n_2+1)$, $n_i = 1/(e^{\hbar\omega_i/k\,T}-1)$. The mode frequencies $\omega_i$ are given in parentheses. The experimental points (○,+,□) represent the corresponding integrated intensities in Figs. 3 and 4.

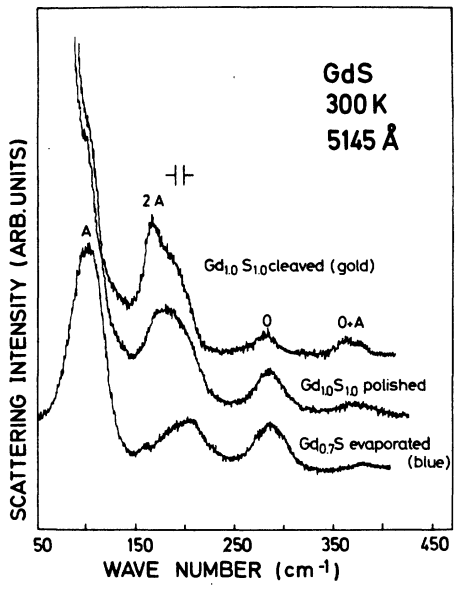


FIG. 7. Comparison of the Raman scattering at 300 K of a cleaved and polished surface of a $Gd_{1.0}S_{1.0}$ single crystal; an evaporated thin film of $Gd_{0.7}S$ is shown for comparison.

defects is very important because of the small penetration depth of the scattering light. The temperature dependence of the *O* band in Figs. 3 and 4 is extremely weak. Its integrated intensity follows very well the calculated Bose factor of a first-order phonon process at, e.g., 280 $cm^{-1}$ as shown by the experimental points (□) in Fig. 6. From the frequency range of the calculated LO phonon branch (225–285 $cm^{-1}$) and TO phonon branch (175–220 $cm^{-1}$) in EuS,[9,15] we presume that the *O* band of $Gd_xS$ ($x = 1.0$, 0.8, 0.7) around 285 $cm^{-1}$ in Fig. 2 corresponds to the one-phonon density of states of optical phonons, most likely from the LO branch. The latter is screened by conduction electrons for wave vectors $|\vec{k}_s|$ smaller than the Thomas-Fermi wave vector

$$|\vec{k}_{TF}| = \left(\frac{12\pi e^2}{(3\pi^2)^{2/3}\hbar^2} \times \frac{n^{1/3}m^*}{\epsilon_\infty}\right)^{1/2}, \qquad (1)$$

where $n$ is the conduction-electron concentration, $m^*$ the effective mass, and $\epsilon_\infty$ the optical dielectric constant. For $Gd_{1.0}S_{1.0}$, with interpolated values $n = 2.33\times10^{22}$ $cm^{-3}$, $m^* = 1.3$, and $\epsilon_\infty = 3.7$ from Ref. 3, we obtain $k_s < k_{TF} = 0.259\times10^8$ $cm^{-1}$ $< k_{max} = \pi/a = 0.565\times10^8$ $cm^{-1}$. Since the *O* band is expected to originate primarily from the high density of states of LO phonons near the zone boundary, we conclude that it is not affected much by screening. Thus, the increase in intensity of the *O* band from $Gd_{1.0}S_{1.0}$ to $Gd_{0.7}S$ is primarily due to the increase in defect concentration. The concurrent decrease in conduction-electron concentration

of about 30% is too small to result in drastic changes in the screening of the LO phonon branch.

Differences in frequency position of the experimentally observed density of states of LO phonons in GdS around 280 $cm^{-1}$ and in EuS around 240 $cm^{-1}$ [9,15] indicate a general trend in $R$-S compounds. The 20% increase in volume compressibility from EuS to SmS has been found to result in a softening of the LO phonon branch near the zone boundary, particularly near the $L$ point.[14] The one-phonon density of states of LO phonons in SmS is found experimentally around 195 $cm^{-1}$,[14] in agreement with a theoretical calculation using the overlap shell model.[9] On the other hand, the TO branch is not strongly affected. A similar comparison between semiconducting EuS and metallic GdS meets with difficulties. However, qualitatively the 50% smaller volume compressibility of GdS compared to EuS is presumably responsible for the 20% increase in frequency position of the LO phonon density of states in GdS.

The zone-center TO phonons of EuS are found experimentally at 178 $cm^{-1}$.[16] The overlap-shell-model calculation for EuS shows the TO branch between 175 $cm^{-1}$ and 220 $cm^{-1}$.[9,15] This branch is not subject to screening by conduction electrons and does not seem to be affected strongly by changes in volume compressibility of $R$-S compounds. Hence, there is a possibility that the density of states of the TO branch and of the screened LO branch near the zone center contribute to the $2A$ band around 200 $cm^{-1}$ as indicated in Figs. 2 and 5.

The $2O$ band around 565 $cm^{-1}$ in Fig. 2 does not depend on the composition of the samples. It is assigned to the allowed second-order RS from optical phonons. Similarly, the intensity of the $O+A$ band in Fig. 2 does not depend on the stoichiometry of the samples either. The only change observed, a smearing of its double-peak structure in $Gd_{1.0}S_{1.0}$ with increasing cation deficiencies, goes in parallel with that in the $A$ band. Because of this fact, we have attributed the $O+A$ band to allowed second-order RS from optical ($O$) and acoustic ($A$) phonons, rather than to 2TO. The latter band should appear at higher frequency (~400 $cm^{-1}$) than the $O+A$ band.

Finally, we would like to concentrate on the structure $2A$ within the gap of acoustic and optical phonons in Fig. 2. While the $A$ band increases strongly in intensity with increasing cation deficiencies, the $2A$ band changes mainly its shape. The $2A$ band shows for $Gd_{1.0}S_{1.0}$ in Fig. 2 a double-peak structure similar to that of the $A$ band, except for reversed order in peak intensity. This double-peak structure disappears with increasing cation deficiencies in the same way as in the $A$ band (Fig. 2). A very similar change in shape of the $2A$ band can be observed by comparing the RS spectra of a cleaved single-crystal surface of $Gd_{1.0}S_{1.0}$ with that of a polished surface as shown in Fig. 7. The double-peak structure in the $2A$ band of the cleaved $Gd_{1.0}S_{1.0}$ single crystal is smeared out after mechanical polishing. Since the polishing introduces additional defects, this smearing parallels the increasing cation deficiencies. From the position in frequency of the $2A$ band and also from the similarity of changes in shape of the $A$ and $2A$ bands with defect concentration, one might suspect that the $2A$ band corresponds to twice the $A$ band. This is indeed confirmed by its temperature dependence in Figs. 3 and 4. The decrease in intensity of the $2A$ band by a factor of 9 from 300 to 10 K is much larger than that of the $A$ and $O$ bands (see Sec. III). The temperature dependence of the integrated intensity of the $2A$ band, as shown by the experimental points (○) in Fig. 6, is in fair agreement with that of the calculated Bose factor, assuming a two-phonon process for the $2A$ band (e.g., $\omega_{1,2}=85$ $cm^{-1}$). The systematically higher values of the experimental points with respect to the calculated Bose factor might be due to a contribution of the one-phonon density of states from the TO branch to the $2A$ band as tentatively indicated in Figs. 2 and 5. However, we conclude that the dominant contribution to the $2A$ band between 140 and 240 $cm^{-1}$ in Figs. 2–5 and 7 is primarily due to allowed second-order RS from acoustic phonons. As a result of our present systematic study as a function of sample composition and temperature, we have to modify somewhat a previously given interpretation.[6] The $2A$ band had been interpreted as originating from TO phonons alone. Changes in the $2A$ and $O$ bands with increasing cation deficiencies had been attributed primarily to changes in the LO-phonon dispersion curve due to screening effects by the varying conduction-electron concentration. Although this effect is not completely negligible, we believe that the change in conduction-electron concentration of our samples (Table I) is too small to compete with the more dominant changes in defect concentration as evidenced by our present experimental findings.

The scattering in GdS is dominated by the contribution of the $A_{1g}+4E_g$ Raman tensor components as shown in Fig. 5. A comparison of the scattering in $x(yz)\bar{x}$ ($T_{2g}$) and $x(z-y,z+y)\bar{x}$ ($3E_g$) configurations from a (100) crystal face of GdS shows the approximate relation $3E_g=2T_{2g}$ over the whole spectral range of Fig. 5. Hence we obtain in Fig. 5 for the contribution in $x(yy)\bar{x}$ configuration $A_{1g}+4E_g \cong A_{1g}+\frac{8}{3}T_{2g}$. Comparing with the $T_{2g}$ spectrum of Fig. 5 we conclude that the $A_{1g}$ component is negligible. Thus the scattering mechanism in GdS is dominated

by the $E_g$ (45%) and $T_{2g}$ (55%) Raman tensor components. The $E_g$ mode symmetry involved for, e.g., the defect-induced one-phonon $O$ band, is a volume-conserving vibration of the S ions with respect to the central Gd vacancy. The volume of the nearest-neighbor S octahedron around a Gd vacancy is conserved for vibrations of opposite S ions, because the S ions are touching one another.

We want to account with a simple model for the defect-induced scattering mechanism as observed for the $O$ band in Fig. 2. The two-phonon process can be viewed as a one-phonon process induced by the "disorder" generated by the second phonon. The defect-induced first-order RS can also be viewed as a second-order process, i.e., one-phonon forbidden scattering mostly by zone-edge phonons induced by the violation in translational symmetry associated with defects. Hence we should be able to compare the scattering intensity of, e.g., the $O$ band with that of the $2O$ band. The $O$ band increases in intensity with Gd vacancies, contrary to the defect-independent $2O$ band.

The scattering intensity $I_2$ of the two-phonon second-order process ($2O$) is given by

$$I_2 \sim |R^{(2)}|^2 \langle u_1^2 \rangle \langle u_2^2 \rangle \tfrac{1}{2} N , \tag{2}$$

where $R^{(2)}$ is the corresponding second-order Raman tensor, $N$ the total number of cells in the crystal, and $\langle u_i^2 \rangle$ the mean square amplitude of the S displacement due to a lattice vibration of frequency $\Omega_i$,

$$\langle u_i^2 \rangle = \frac{\hbar (n_B + 1)}{4MN\Omega_i} , \tag{3}$$

with $n_B$ the Bose factor and $M$ the reduced mass of the diatomic lattice, $2/M = 1/M_1 + 1/M_2$.

For the one-phonon impurity-induced process ($O$) we replace $\langle u_2^2 \rangle$ in Eq. (2) by the temperature-independent disorder-induced fluctuation in the atomic positions $\langle r^2 \rangle$:

$$I_d \sim |R^{(2)}|^2 \langle u_1^2 \rangle \langle r^2 \rangle N_d . \tag{4}$$

For cation vacancies $\langle r^2 \rangle$ is mainly the mean square defect-induced displacement of the S ions from their equilibrium position at zero temperature and $N_d$ is the total number of such defects. For the intensity ration $I_2/I_d$ of the $2O$ and $O$ processes we obtain

$$I_2/I_d = \tfrac{1}{2} \langle u_2^2 \rangle N / \langle r^2 \rangle N_d . \tag{5}$$

$I_2$ can be calculated using the above formula for $\langle u_i^2 \rangle$, $\Omega_i = 280$ cm$^{-1}$ from Fig. 2 and $M = 53.2$. The major problem consists in an estimate of $\langle r^2 \rangle$. In first approximation, a Gd vacancy in $Gd^{3+}S^{2-}$ corresponds to a lack of charge transfer of two valence electrons from Gd to S. Hence, instead of a $S^{2-}$ ion of radius 1.84 Å we have a neutral S atom of radius 1.27 Å. A total change in S radius of 0.57 Å occurs. In a local description we consider the octahedron of six nearest S neighbors around a Gd vacancy. Hence each S ion is affected by only $\frac{1}{6}$ of the above charge transfer, resulting in a reduction in radius of $\Delta r = \frac{1}{6} \times 0.57$ Å.

It is reasonable to assume that the defect-induced displacement of each S ion is proportional to $\Delta r$. The amplitude in the direction of the central Gd vacancy is $\Delta r/\sqrt{2}$, because the $S^{2-}$ ions are touching one another along the line connecting their centers. We obtain

$$\langle r^2 \rangle = (\Delta r/\sqrt{2})^2 \times 1/N \times 6 , \tag{6}$$

where $1/N$ is a normalizing factor and the factor 6 considers the effect of one vacancy on six neighboring S ions. Hence we can calculate $I_d$ for, e.g., $Gd_{0.8}S$ with $N_d = 0.2N$. Finally, we obtain from our model a ratio $I_2/I_d = 0.07$ for $Gd_{0.8}S$. Taking into account the above simplified assumptions, this result agrees fairly well with the experimental observation of $I_2/I_d = 0.1$ for $Gd_{0.8}S$ in Fig. 2.

Our present experiments on GdS have not provided any evidence of spin-dependent phonon RS with the onset of antiferromagnetic order, contrary to EuSe,[13] and EuTe.[8,9] We believe that this has to be associated with the fact that the $4f$ states around 7 eV below $E_F$ are not resonantly excited by the 2.4–2.7 eV laser excitations used. This fact is presumably also responsible for the lack of two-magnon scattering. Without resonant excitation of the magnetic $4f$ states, the exchange-scattering mechanism for two-magnon scattering in antiferromagnets[17] seems to be inoperative. On the other hand, one-magnon scattering of GdS is expected to occur at very low frequencies since the magnon energy at $\vec{k} \sim 0$ depends only on the anisotropy field. The latter is very small for the spherically symmetric $^8S_{7/2}$ ground state of $Gd^{3+}$. Hence the one-magnon scattering will be hidden underneath the strong Rayleigh tail below 50 cm$^{-1}$ in Figs. 3 and 4. In addition, it will be resonantly enhanced only around 4 eV,[18] due to the $^8S_{7/2} \rightarrow {}^6P_J$ transition.[17] In the present case of GdS resonant enhancement is expected to occur for transitions from the $4f^7$ states to empty $5d$ states above $E_F$ for photon energies $\hbar\omega > 7$ eV.

It is of particular interest to mention the striking similarity between the Raman spectra of GdS and those of superconducting transition-metal compounds, such as TiN, ZrN, and NbC.[19] The latter group of materials exhibits also a pronounced defect structure and a plasma reflection edge in the visible region of the spectrum. One also observes, as in GdS, a defect-induced first-order RS and allowed RS of second order. The only differences

concern a partial overlap of the $2A$ and $O$ bands and a systematic shift of the phonon modes to higher frequencies because of the lighter cation and anion masses in these transition-metal compounds. In GdS superconductivity is suppressed due to the $Gd^{3+}(^8S_{7/2})$ magnetic moment of $7\mu_B$. However, LaS, which has no occupied $4f$ states, represents the isoelectronic and superconducting ($T_C = 0.84$ K)[3] counterpart of GdS. Hence the study of Raman scattering in LaS appears to be an interesting project for future work.

## V. CONCLUSION

Our RS experiments on GdS have provided important information about phonons which is otherwise not accessible. By performing investigations as a function of sample stoichiometry and temperature we were able to identify defect-induced first-order scattering from acoustic and optical phonons with respect to allowed second-order RS.

Since the localized $4f$ states of GdS have not been resonantly excited by the laser lines used, the effects of spin-disorder-induced scattering or spin-dependent phonon RS, as observed in EuX, are absent. This in turn emphasizes the important role of the localized $4f$ levels as initial states in RS of EuX and SmS. The first-order RS of GdS is seen to be dominated by defects rather than by concurrent changes in conduction-electron concentration. The defect-induced RS of GdS provides a sensitive measure of the stoichiometry of the samples. Comparison with light-scattering experiments on other NaCl-type transition-metal compounds indicates a general trend for the scattering mechanism and the phonons observed in this class of cubic materials.

*Note added in proof.* While proofreading this paper the results of neutron scattering of YS came to our attention [P. Roedhammer (private communication); P. Roedhammer, W. Reichardt, W. Weber and F. Holtzberg, Int. Conf. on Lattice Dynamics, Paris, 1977 (unpublished)]. Neutron scattering of superconducting *YS* indicates that the TO, LO branches are flat and practically overlap each other, thus implying an essentially zero TO-LO splitting at the zone boundary. At first sight, this result appears to be opposite to our tentatively assigned TO-LO splitting in Figs. 2 and 5. Although we cannot exclude similar dispersion curves for antiferromagnetic GdS (neutron scattering data are not as yet available), one should consider that there may well be a difference in the electron-phonon coupling of these two compounds. We feel that this point deserves further independent investigations.

## ACKNOWLEDGMENT

The authors would like to express their gratitude to Professor H. Bilz for many fruitful and stimulating discussions. We would like to thank Mr. K. Fischer for growing the single crystals, Dr. K. Reichelt for performing the electron microscope investigations, and Dr. T. P. Martin and Dr. G. Winterling for helpful cooperation. We are obliged to T. P. Martin for criticism of the work.

---

*Institut für Festkörperforschung, Kernforschungsanlage Jülich, Federal Republic of Germany.

†Permanent address: National Technical University, Athens, Greece.

[1]F. Holtzberg, D. C. Cronemeyer, T. R. McGuire, and S. von Molnar, U. S. Natl. Bur. Stand. No. Spec. Publ. 364 (U.S. GPO, Washington, D. C., 1972), p. 637.

[2]G. Güntherodt and P. Wachter, AIP Conf. Proc. 18, 1034 (1973).

[3]W. Beckenbaugh, J. Evers, G. Güntherodt, E. Kaldis, and P. Wachter, J. Phys. Chem. Solids 36, 239 (1975).

[4]G. E. Bacon, *Neutron Diffraction*, 3rd ed. (Clarendon, Oxford, 1975).

[5]J. Flahaut and P. Laruelle, Prog. Sci. Technol. Rare Earths 3, 149 (1968).

[6]E. Anastassakis, H. Bilz, M. Cardona, P. Grünberg, and W. Zinn, in *Light Scattering in Solids*, edited by M. Balkanski *et al.* (Flammarion, Paris, 1976), p. 367.

[7]N. Suzuki and H. Kamimura, J. Phys. Soc. Jpn. 35, 985 (1973).

[8]G. Güntherodt, *Proceedings of the 13th International Conference on the Physics of Semiconductors, Rome,* 1976, edited by F. G. Fumi (Tipografia Marves, Rome, 1976), Güntherodt, p. 291.

[9]P. Grünberg, G. Güntherodt, R. Merlin, A. Frey, W. Kress, H. Bilz, M. Cardona, K. Fischer, and W. Zinn (unpublished).

[10]G. Güntherodt, *Advances in Solid State Physics*, edited by J. Treusch (Vieweg, Braunschweig, 1976), Vol. XVI, p. 95.

[11]D. E. Eastman and M. Kuznietz, J. Appl. Phys. 42, 1396 (1971).

[12]D. E. Eastman, F. Holtzberg, J. L. Freeouf, and M. Erbudak, AIP Conf. Proc. 18, 1030 (1973).

[13]R. P. Silberstein, L. E. Schmutz, V. J. Tekippe, M. S. Dresselhaus, and R. L. Aggarwal, Solid State Commun. 18, 1173 (1976).

[14]G. Güntherodt, R. Keller, P. Grünberg, A. Frey, W. Kress, R. Merlin, W. B. Holzapfel, and F. Holtzberg, in *Proceedings of the International Conference on Valence Instabilities and Related Narrow Band Phenomena, Rochester, 1976* (Plenum, New York, 1977), p. 321.

[15]P. Grünberg, G. Güntherodt, A. Frey, and W. Kress,

Physica B 89, 225 (1977).
[16]J. D. Axe, J. Phys. Chem. Solids 30, 1403 (1969).
[17]P. A. Fleury and R. Loudon, Phys. Rev. 166, 514 (1968).
[18]G. H.Dieke, H. M. Crosswhite and B. Dunn, J. Opt. Soc. Am. 51, 820 (1961).
[19]W. Spengler, R. Kaiser, and H. Bilz, Solid State Commun. 17, 19 (1975); W. Spengler and R. Kaiser, *ibid.* 18, 881 (1976).